# High precision difference astrometry applied to the triplet of S5 radio sources B1803+784/Q1928+738/B2007+777

E. Ros[*1], J.M. Marcaide[1], J.C. Guirado[1], M.I. Ratner[2], I.I. Shapiro[2], T.P. Krichbaum[3], A. Witzel[3], and R.A. Preston[4]

[1] Departament d'Astronomia i Astrofísica, Universitat de València, E-46100 Burjassot, València, Spain
[2] Harvard-Smithsonian Center for Astrophysics, 60 Garden St., Cambridge, MA 02138, USA
[3] Max-Planck-Institut für Radioastronomie, Auf dem Hügel 69, D-53121 Bonn, Germany
[4] Jet Propulsion Laboratory, California Institute of Technology, 4800 Oak Grove, Pasadena, CA 91109, USA

**Abstract.** We determined the separations of the radio sources in the triangle formed by the BL Lac objects 1803+784 and 2007+777, and the QSO 1928+738 from intercontinental interferometric observations carried out in November 1991 at the frequencies of 2.3 and 8.4 GHz simultaneously. Difference phase-delay astrometry yielded the following separations:

$$\Delta\alpha_{(1803+784)-(1928+738)}=-1^h27^m\ 2\overset{s}{.}811256\pm0\overset{s}{.}000062$$
$$\Delta\delta_{(1803+784)-(1928+738)}=\ 4°\ 30'\ 2\overset{''}{.}44833\ \pm0\overset{''}{.}00012$$
$$\Delta\alpha_{(1928+738)-(2007+777)}=-0^h37^m42\overset{s}{.}503305\pm0\overset{s}{.}000033$$
$$\Delta\delta_{(1928+738)-(2007+777)}=-3°\ 54'41\overset{''}{.}67756\ \pm0\overset{''}{.}00013$$
$$\Delta\alpha_{(2007+777)-(1803+784)}=\ 2^h\ 4^m45\overset{s}{.}314561\pm0\overset{s}{.}000052$$
$$\Delta\delta_{(2007+777)-(1803+784)}=-0°\ 35'20\overset{''}{.}77077\ \pm0\overset{''}{.}00013$$

We successfully connected differenced phase delays over 7° on the sky at 8.4 GHz at an epoch of maximum solar activity. The effects of the ionosphere on these VLBI data were mostly removed by estimates of the total electron content from observations of GPS satellites. The comparison of the estimated separation of QSO 1928+738 and BL 2007+777 with previous such estimates obtained from data at different epochs leads us to a particular alignment of the maps of QSO 1928+738 at different epochs relative to those of BL 2007+777, although with significant uncertainty. For this alignment, that the jet components of QSO 1928+738 show a mean proper motion of 0.32±0.10 mas/yr and also suggest an identification for the position of the core of this radio source.

**Key words:** techniques: interferometric – astrometry – galaxies: BL Lacertae objects: individual: B1803+784; B2007+777; Q1928+738

## 1. Introduction

A key need of astronomers is a celestial reference frame. Initially they used optical observations to obtain such a reference frame (see, e.g., Fricke et al. 1988, Fricke et al. 1991). A more

rigid and accurate frame can be obtained using Very Long Baseline Interferometry (VLBI), a technique that provides far higher angular resolution (see, for example, Johnston et al. 1995). Using differenced phase delays from observations of two sources yields relative positions of radio sources with submilliarcsecond accuracy and fractional precisions reaching $\sim 2 \cdot 10^{-9}$ (Guirado et al. 1995a, 1995b, Lara et al. 1996). Differenced phase delays may provide the most precise observable in astrometry. The group-delay observable, although also capable of providing global astrometry, has a statistical standard error larger than the phase-delay error by a factor equal to the ratio of the center frequency of the VLBI observations to their effective bandwidth.

In radio astrometric work, it is important to account for the propagation medium, including the ionosphere. Sardón et al. (1994) showed that the total electron content (TEC) of the ionosphere could be determined with high accuracy (standard error of about 2%) for all directions from a site by using dual-frequency GPS data. The ionospheric contribution can also be determined from dual-band VLBI observations by comparing connected phase delays (or group delays) from the two bands. In this paper, we compare those approaches for estimating the effect of the ionosphere.

Our use of a triangle of targets allows an improvement with respect to astrometry with pairs of radio sources (e.g., Guirado et al. 1995a, 1995b, 1998): closure on the sky provides a check on the internal consistency of the data reduction.

## 2. VLBI observations and data analysis

We observed the radio sources BL 1803+784, QSO 1928+738, and BL 2007+777 in right circular polarization at both 2.3 and 8.4 GHz, on 20 and 21 November 1991 (MJD 48580 and 48581) from 14:00 to 04:00 UT. Using a global VLBI array, we recorded with the Mark III system (Rogers et al. 1983), in modes A (56 MHz) or B (28 MHz), depending on the instrumentation at the individual sites. The array consisted of the following antennas (in parenthesis, code, diameter, location): Effelsberg (B, 100 m, Germany); Haystack (K, 37 m, Massachusetts, US); Medicina (L, 32 m, Italy); DSS63 (M, 70 m, Spain); and phased-VLA (Y, 130 m effective diameter, New Mexico, US); Fort

*Send offprint requests to*: E. Ros (ros@mpifr-bonn.mpg.de)
[*] *Present address:* Max-Planck-Institut für Radioastronomie, Auf dem Hügel 69, D-53121 Bonn, Germany

Davis (F, 25 m, Texas, US); Kitt Peak (T, 25 m, Arizona, US); Pie Town (P, 25 m, New Mexico, US); Los Alamos (X, 25 m, New Mexico, US); and Green Bank (G, 43 m, West Virginia, US).

The three radio sources were observed cyclically (cycle time of 9 min, clockwise direction) with 2 minutes "on" radio source and 1 minute allowed for slewing antennas. All sources had total flux densities greater than 1 Jy at the epoch of observation. We obtained strong detections from each of the baselines for at least 80% of the 2 min "scans".

The observations were plagued by problems. Medicina and Green Bank had phasing problems. DSS63 recorded only 3 hours of data. The phased-VLA recorded only 8.4 GHz data, and Haystack was set to a wrong sky frequency. After many fruitless attempts to use part of the data from these stations, we decided to use only the data from the subset of antennas with very good performance: Effelsberg, Fort Davis, Pie Town, Kitt Peak, and Los Alamos.

The data were correlated at the Max-Planck-Institut für Radioastronomie, Bonn, Germany. After fringe-fitting the correlator output, we obtained for each observation and baseline, estimates of the group delay, the phase-delay rate, the fringe phase (modulo $2\pi$), and the correlation amplitude at each of two selected reference frequencies (2,294.99 MHz and 8,404.99 MHz). Following standard procedures we constructed the visibilities using the calibration information provided by staff of the antennas. We made hybrid maps of each of the three radio sources at 2.3 and 8.4 GHz using the Caltech package (Pearson 1991) and DIFMAP (Shepherd et al. 1995). Our mapping results are presented in Sect. 3 and our astrometric results in Sects. 4 and 5.

## 3. Mapping of the radio sources BL 1803+784, QSO 1928+738, and BL 2007+777

A complete sample (S5) (Kühr et al. 1981) of compact radio sources has been studied using the VLBI technique over the last two decades (Eckart et al. 1986, 1987, Witzel et al. 1988). These sources were selected from the fifth installment of the MPIfR-NRAO 5 GHz strong source survey. The sources have flat spectra that permit multiband observations. All members of this sample have neighbors relatively nearby on the sky, allowing phase-reference observations to be made (Guirado et al. 1995a, 1998).

### 3.1. The BL Lac object 1803+784

1803+784 is a BL Lacertae type object with $z$=0.684 and $V$=16.4 (Stickel et al. 1991). It exhibits a radio structure with kiloparsec-size components (Antonucci 1986, Strom & Biermann 1991, Kollgaard et al. 1992, Murphy et al. 1993) to the south of the core (at angular distances from the core of 2″, 37″ and 45″). On parsec scales the source shows a westward jet (Eckart et al. 1986, Pearson & Readhead 1988, Schalinski 1990); VLBI monitoring of these milliarcsecond (mas)-size components at 22 GHz shows components at angular distances of about 0.4, 1.4 and 5 mas from the core (Eckart et al. 1986,
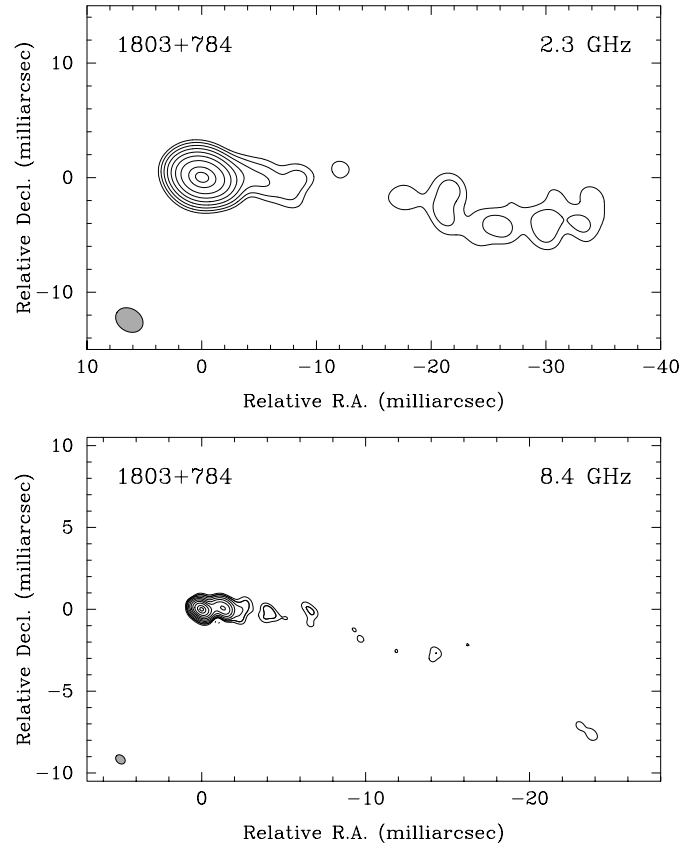


**Fig. 1.** Hybrid maps from observations on 20-21 November 1991 of the BL Lacertae object 1803+784 at 2.3 and 8.4 GHz. Contours are 0.5, 1, 2, 4, 8, 16, 32, 64, and 90% of the peak of brightness, 1.78 Jy/beam, for 2.3 GHz, and –0.25, 0.25, 0.5, 1, 2, 4, 8, 16, 32, 64, and 90% of the peak of brightness, 1.40 Jy/beam, for 8.4 GHz. Dotted lines correspond to negative contours. The size of the natural restoring beam, shown at the bottom left corner of each map, is $2.53 \times 1.97$ mas (PA=58°) for 2.3 GHz and $0.65 \times 0.49$ mas (PA=49°) for 8.4 GHz. Note that the scales of the two maps are not the same.

Schalinski 1990, Krichbaum et al. 1990, 1993, 1994a, 1994b). Observations at 22 and 43 GHz also reveal other features that appear to be moving between the core and the 1.4 mas component. Steffen (1994) has modeled this radio source as an adiabatically expanding homogeneous plasma jet moving along a helical trajectory. The parsec-scale structure is misaligned with the kiloparsec structure by ∼90°.

In our maps (see Fig. 1), we find well defined components to the west of the core, with the jet structure extending up to 35 mas from the core at 2.3 GHz and up to 21 mas at 8.4 GHz. The features in our maps agree well with those shown in previous maps.

### 3.2. The QSO 1928+738 (4C 73.18)

QSO 1928+738, also known as 4C 73.18, is a well-studied quasar with $z$=0.302 and $V$=15.5 (Lawrence et al. 1986). On kiloparsec scales, it exhibits two-sided jet emission feeding two symmetrically placed lobes in a north-south orientation (Rusk &
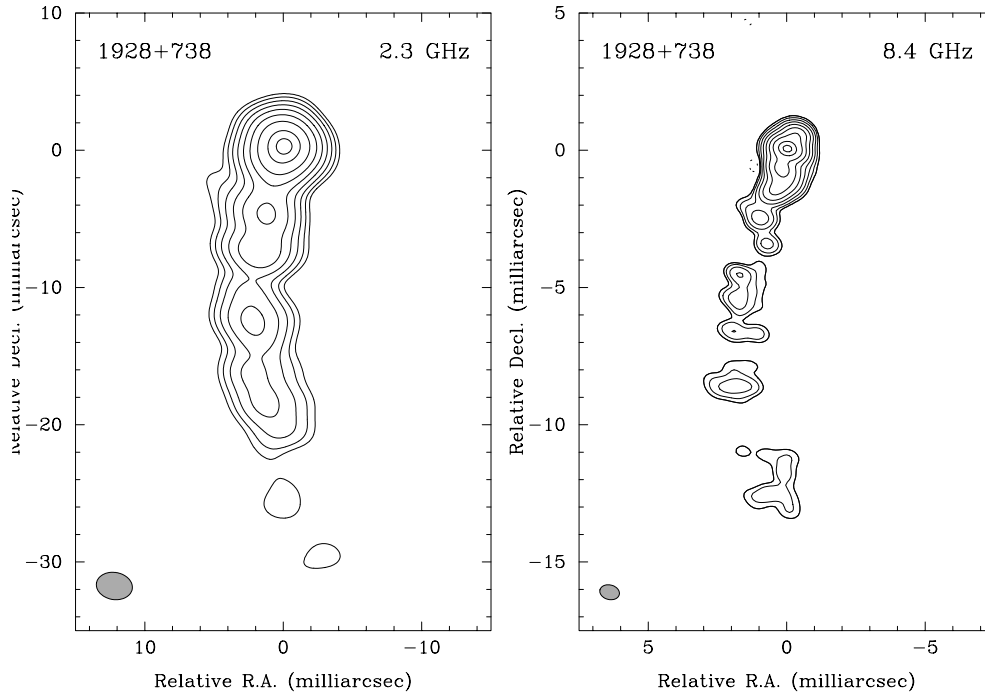
**Fig. 2.** Hybrid maps from observations on 20-21 November 1991 of the QSO 1928+738 (4C 73.18) at 2.3 and 8.4 GHz. Contours are 0.5, 1, 2, 4, 8, 16, 32, 64, and 90% of the peak of brightness, 1.16 Jy/beam, for 2.3 GHz, and –0.5, 0.5, 1, 2, 4, 8, 16, 32, 64, and 90% of the peak of brightness, 1.18 Jy/beam, for 8.4 GHz. Dotted lines correspond to negative contours. The size of the natural restoring beam, shown at the bottom left corner of each map, is 1.98×2.62 mas (PA=80°) for 2.3 GHz and 0.72×0.53 mas (PA=76°) for 8.4 GHz. Note that the scales of the two maps are not the same.

Rusk 1986, Johnston et al. 1987, Murphy et al. 1993). On parsec scales it displays a pronounced one-sided southward jet with superluminal motion along a sinusoidally curved jet (Eckart 1985, Pearson & Readhead 1988, Hummel 1990, and Hummel et al. 1992, hereafter H92). H92 describe this source as having a helical magnetic field attached to a rotating accretion disk. Further, Roos et al. (1993) suggest that the source consists of two massive black holes, with mass ratio smaller than 10, total mass $\sim10^8 M_\odot$ and orbital radius $\sim10^{16}$cm. Such massive binary black holes could be responsible for the sinusoidal jet ridge line which has a period of precession of about 2.9 years according to the ballistic relativistic jet model.

Our maps (see Fig. 2) show the core-jet structure, with components in the jet up to 30 mas south of the core at 2.3 GHz and up to 13 mas south at 8.4 GHz.

### 3.3. The BL Lac object 2007+777

2007+777 is also a BL Lacertae type object with $z$=0.342 and $V$=16.5 (Stickel et al. 1991). It is a core-dominated radio source with a westward-directed jet of parsec scale with superluminal components discernible up to 6 mas from the core (Eckart 1983). This source has also been studied on a kiloparsec scale (Antonucci 1986, Kollgaard et al. 1992). The kiloparsec structure is aligned with the parsec structure and has components $\sim11''$ east of the core, and a jetlike feature extending $16''$ to the west with components at $\sim8.5''$ and $\sim15.8''$ from the core.

For this source our maps (see Fig. 3) show a relatively small jet extending 8 mas west of the core. We identify the brightest component of the map as the core due to its spectral power being the same at 2.3 GHz and 8.4 GHz.

## 4. Astrometric data reduction

Our astrometric data reduction contains several steps which yield nearly "ionosphere-free" and "structure-free" phase-connected delays. Using an extensively modernized version of software originally written by Robertson (1975), we analyze these delays via weighted least-squares to estimate the angular separations among the sources. In the next paragraphs we discuss in detail each of the steps of this process.

### 4.1. Phase connection

We used the 8.4 GHz group delays, $\tau_g$, together with the phase-delay rates, $\dot{\tau}_\phi$, to estimate via weighted-least-squares the values of the parameters of our theoretical models including the behavior of the atomic clock at each site relative to that at a reference site. Using this astrometric model we predicted for each of our ten baselines the number of cycles of phase between successive observations of the same source to permit us to "connect" the phase delays (Shapiro et al. 1979). Denoting the reference frequency (8,404.99 MHz) by $\nu_r$ and the cycle time of the observations (9 min) by $\Delta t$, we can represent the constraint on the standard error, $\sigma(\dot{\tau}_\phi)$, needed to insure proper phase connection: $\sigma(\dot{\tau}_\phi) \ll (\nu_r \Delta t)^{-1}$, i.e., $\sigma(\dot{\tau}_\phi)$ must be small compared to $0.2\,\mathrm{ps}\cdot\mathrm{s}^{-1}$. In our observations, this criterion is satisfied at 8.4 GHz for our observations and essentially complete phase connection was feasible. However, phase connection was not possible for the data at 2.3 GHz, due to the strong effect of the ionosphere and the consequent high scatter in the phase-delay data, leading to a violation of the criterion stated above.

We also considered possible overall offsets (equivalent to an integral number of cycles of phase for all the baselines involving a given site and source, i.e., constant clock offsets or fringe

**Table 1.** Parameters of the theoretical model used in the weighted-least-squares analysis.

**Source coordinates (J2000.0)[a]**

1928+738[b]       $\alpha = 19^h 27^m 48\overset{s}{.}495213$       $\delta = 73°58'01\overset{''}{.}56995$

**Antenna site coordinates and propagation medium parameters[a,c]**

| Radio telescopes[d] | Cartesian coordinates [m] | | | Axis offset[e] [m] | Mean tropospheric zenith delay[f] [ns] | |
|---|---|---|---|---|---|---|
| | X | Y | Z | | $\tau_{dry}$ | $\tau_{wet}$ |
| B | 4033947.528 | 486990.428 | 4900430.727 | 0.0 | 7.4 | 0.2 |
| F | −1324009.072 | −5332181.961 | 3231962.515 | 2.123 | 6.4 | 0.4 |
| P | −1640953.650 | −5014816.009 | 3575411.928 | 2.136 | 5.9 | 0.1 |
| T | −1995678.575 | −5037317.707 | 3357328.183 | 2.138 | 6.2 | 0.0 |
| X | −1449752.303 | −4975298.589 | 3709123.975 | 2.139 | 6.2 | 0.0 |

**Earth Tides**

Radial Love number, **h**=0.60967       Horizontal Love number, **l**=0.085       Tidal lag angle, $\theta = 0\overset{\circ}{.}0$

**Earth Orientation Parameters[a]**

| **Nutation** | **Polar Motion and UT1** | **Precession Constant (J2000.0)[g]** |
|---|---|---|
| IAU 1980 Nutation Series + | Wobble: **x**=0$\overset{''}{.}$25221 **y**=0$\overset{''}{.}$27880 | p=5029$\overset{''}{.}$0966/Julian century |
| IERS corrections for MJD=48580: | IERS LOD correction= $0.002422s$ | **Mean obliquity (J2000.0)[g]** |
| $d\psi = -0\overset{''}{.}01238 \; d\epsilon = -0\overset{''}{.}00201$ | UT1-UTC= $-0.027891s$ | $\epsilon_0$=23°26'21$\overset{''}{.}$448=84381$\overset{''}{.}$448 |

[a] The reference coordinates are taken from 1993 IERS Annual Report (IERS 1994); they are used only for convenience. We used standard deviations from the IERS parameter estimates, but increased them twofold to be conservative. These increased standard deviations are: 0.035 ms and 0.28 mas for the $(\alpha, \delta)$ QSO 1928+738 coordinates, 2 cm in each coordinate of site position, 1 mas in each pole coordinate, and 0.04 ms in UT1-UTC. See Table 3.

[b] The position of QSO 1928+738 was held fixed and the positions of the other two sources were determined with respect to it.

[c] The site positions were calculated by linear extrapolation (using the constant velocities for the coordinates obtained from IERS (1994) and applied to its 1993.0 positions).

[d] See text for key.

[e] All the antennas are altitude-azimuth.

[f] Mean values of the zenith delays, computed using the meteorological values provided by the staff of the observing antennas (see, e.g., Saastamoinen 1973).

[g] Lieske et al. (1977).

ambiguity offsets). To estimate such possible offsets, we considered the fringe ambiguity offsets as parameters whose values were to be estimated and we introduced one of them into the global weighted-least-squares analysis for each site for each radio source. The values obtained were all less than 24 ps, a fifth of an ambiguity interval. We concluded that the fringe ambiguity offsets for the phase-delay data at 8.4 GHz are all zero.

### 4.2. Radio source structure correction

The selection of the reference point in each map is a critical task. The meaningful accuracy of our final sky-position estimate can be no better than the accuracy with which we can identify a specific "physical" reference point in our map. Using the Caltech package (Pearson 1991), we made special renditions of the images of our radio sources with a pixel size of 0.01 mas for 8.4 GHz (about 70 times smaller than the size of the CLEAN beam). For Figs. 1–3, the delta-function components from the CLEAN procedure had been convolved with the corresponding Gaussian beams. For these special renditions of the images we also convolved the CLEAN components with their corresponding Gaussian beams. We chose as the reference point the center of the pixel corresponding to the peak of the brightness distri-

bution, for each radio source and frequency. For a source with a "sharp" peak, the standard error in this location is proportional to the ratio between the size of the interferometric beam and the SNR of the peak of brightness in the map (see, for example, Fomalont 1989). Using our reference points, we calculated the structure contributions to the phase delay. None of the contributions is larger than 25 ps. Thus, the structure contributions at 8.4 GHz are ∼0.2 cycles (no more than 70°) for QSO 1928+738, the source with the largest structure.

Another choice (see Guirado et al. 1995a) of reference point is the centroid of those delta-function components with flux densities larger than 25% of the component with the highest flux density, in the area covered by the "main lobe" of the synthesized beam. The difference in the positions determined from these two criteria is $\leq 20\,\mu$as.

### 4.3. Troposphere correction

The neutral atmosphere introduces a delay $\tau_{atm}$ in the optical path length of the radio wave of about 2.3 m in the zenith direction. From meteorological data obtained at each antenna site, we calculated (see, e.g., Saastamoinen 1973) a priori values for
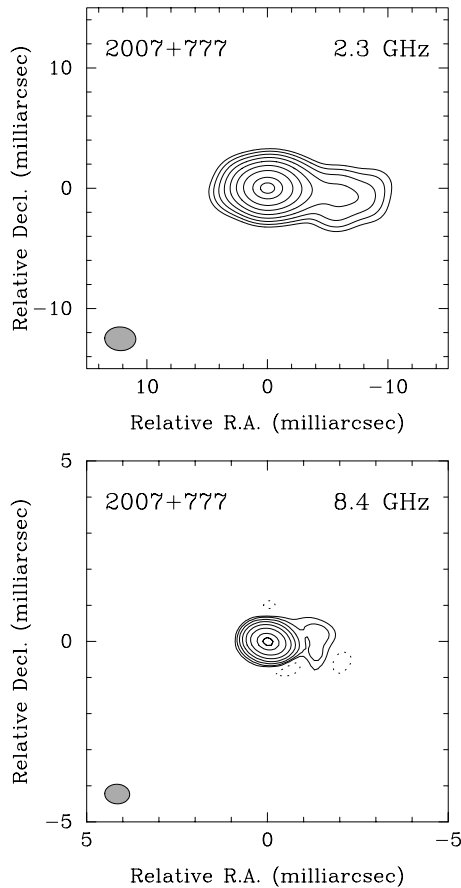
**Fig. 3.** Hybrid maps from observations on 20-21 November 1991 of the BL Lacertae object 2007+777 at 2.3 and 8.4 GHz. Contours are 0.5, 1, 2, 4, 8, 16, 32, 64, and 90% of the peak of brightness, 0.69 Jy/beam, for 2.3 GHz, and –1, 1, 2, 4, 8, 16, 32, 64, and 90% of the peak of brightness, 2.06 Jy/beam, for 8.4 GHz. Dotted lines correspond to negative contours. The size of the natural restoring beam, shown at the bottom left corner of each map, is 2.58×1.97 mas (PA=87°) for 2.3 GHz and 0.69×0.54 mas (PA=87°) for 8.4 GHz. Note that the scales of the two maps are not the same.

the two components of the delay at local zenith: the dry and the wet. We show these values in Table 1.

For the weighted-least-squares analysis, we represented the zenith delay as a continuous, piecewise-linear function of time and determined it from meteorological values sampled every two hours during the observation. We used the Chao mapping function (Chao 1972, 1974) to approximate the delay at elevation angles other than the zenith. These angles were always greater than 20°, and for these delays the Chao mapping function yields results consistent with those from other more accurate mapping functions.

### 4.4. Ionosphere correction

The plasma delay due to the Earth's ionosphere was the most difficult contribution to estimate. With observations made at two frequency bands simultaneously, the ionospheric contribution can largely be removed from some observations by taking

advantage of the $\nu^{-2}$ dependence of the effect. The delay of a radio wave propagating through a (weak) plasma can be approximated by: $\Delta\tau_{ion} = \pm(kE_c)/(c\nu^2)$ (see, for example, Thompson et al. 1986), where $k$=40.3 m$^3$s$^{-2}$, $c$ is the speed of light (m·s$^{-1}$), $\nu$ the frequency (Hz), and $E_c$ the integrated electron content (m$^{-2}$) along the line of sight; the plus and minus signs refer to group and phase delays, respectively. Unfortunately, for our observations, which were made near a maximum in solar activity, we could not phase connect the delays at 2.3 GHz, as noted in Sect. 4.1. Although the group-delay data at 2.3 GHz and at 8.4 GHz can be combined to yield ionospheric corrections, these are not accurate enough to allow us to phase connect the 2.3 GHz delay data.

Because we believed the corrections for the ionosphere would be somewhat more accurate, we used estimates of $E_c$ from Global Positioning System (GPS) data (Sardón et al. 1994) instead of from the dual-band VLBI data. The GPS system uses two frequency bands, one each at 1,575.42 MHz and 1,227.60 MHz. From data obtained simultaneously at one site from different satellites, we estimated the total electron content in the zenith direction. With such estimates from a number of sites, together with our model of the electron distribution in the ionosphere, we can interpolate to obtain the delay in a given direction for a given (relatively nearby) site (see Klobuchar 1975). We therefore obtained data from several GPS stations for the time span of our observations. For the U.S. part of the array we used the TEC data from Goldstone (CA, US, 116.890°W, 35.426°N) and Pinyon Flats (CA, US, 116.458°W, 33.612°N) available at the GARNER archives at SOPAC, University of California-San Diego, to estimate the TEC for each of our VLBI observations for the following antennas: Fort Davis (103.944°W, 30.635°N), Pie Town (108.119°W, 34.301°N), Kitt Peak (111.612°W, 31.956°N), and Los Alamos (106.245°W, 35.775°N), in each case introducing a longitude (time) correction and an appropriate "slant" factor. In our relatively crude procedure, following the geometry from Klobuchar (1975), we assumed that the TEC was concentrated at an altitude of 350 km. To determine the TEC for Effelsberg (6.844°E, 50.336°N), we used the data from Herstmonceux (UK, 0.336°E, 50.867°N) and Wettzell (Koetzling, Germany, 12.789°E, 49.144°N) obtained from the archives mentioned above. Further details will be provided in Ros et al. (1999). We used the GPS results as described above to deduce ionosphere corrections for the line of sight from each VLBI station to each radio source for each scan, and to thereby correct the group delays (at both frequencies) and phase delays (at 8.4 GHz). The corrections were as large as 10 turns (cycles) at 8.4 GHz for some scans on intercontinental baselines. The statistical standard errors of the GPS corrections at 8.4 GHz are 30 ps, a fourth of an ambiguity interval, corresponding to a TEC standard error of $1.5\times10^{16}$ el/m$^2$.

### 4.5. Differenced observables

After the phase-connected observables at 8.4 GHz for each source were corrected for source structure and ionospheric ef-

fects, we formed the differenced phase delays by subtracting the phase delay of each observation of a radio source of the triangle from the previous one observed in the cycle. The differenced phase delays are thus partially free from unmodeled effects that remain in the phase delays for each one of the sources, such as those effects due to instabilities of the time standards used at the sites and inadequacies in the modeling of the troposphere. When working with sources nearby to one another on the sky, subtraction of results from consecutive observations tends to cancel errors since the received signals from the two sources follow similar paths at nearly the same epochs. With sources at larger angular separations, such tendencies to cancel are weaker: not only are the spatial separations of the ray paths larger, but the epochs of successive observations tend to be further apart, due to the limited slew speeds of the antennas. In our case the source separations range from $4°$ to $7°$.

Next, the undifferenced and differenced phase-delay data from the three radio sources were used in a weighted-least-squares analysis (the use of different subsets of data, e.g., undifferenced data from only one or two of the three radio sources, or the use of two or three sets of differenced data does not alter the results or the statistical standard errors significantly). We included undifferenced observables to better estimate the long-term behavior of the station clocks. For each baseline, we scaled separately the standard deviations of the undifferenced phase delays for each radio source and the differenced phase delays for each pair of radio sources to give a root-weighted-mean-square of unity for the corresponding set of postfit residuals. The resulting undifferenced phase delays have about threefold larger standard errors than do the differenced phase delays.

At this stage of the data reduction we again checked for possible nonzero fringe ambiguity offsets and possible errors in phase connection. Estimating the fringe ambiguity offsets in a least-squares analysis again yielded small values (a few picoseconds), showing that no changes were necessary.

## 5. Angular separations

With these phase-connected, nearly ionosphere- and structure-free phase-delay data, we estimated the angular separations among the pairs of radio sources of the triangle. Specifically, we estimated the coordinates of BL 1803+784 and BL 2007+777 with respect to the fixed coordinates of QSO 1928+738. We used the data of the three radio sources jointly to obtain these solutions. The results are shown on Table 2 and the postfit residuals of the differenced phase delays in Fig. 4.

We did not estimate in the weighted-least-squares analyses the tropospheric zenith delays, the site coordinates, the coordinates of the reference source (i.e., QSO 1928+738; using either of the other two sources as reference does not alter the results significantly), the coordinates of the Earth's pole, and UT1-UTC. Instead, to accommodate software limitations we fixed their values equal to their a priori values (see Table 1), and accounted for their a priori standard errors in our subsequent sensitivity analysis (see Table 3). For each solution of the angular separations we estimated the overall standard errors of the

**Table 2.** Relative right ascensions and declinations in J2000.0 coordinates of the radio sources BL 1803+784, QSO 1928+738 and BL 2007+777, labeled as A, B, and C, respectively, obtained by a weighted-least-squares analysis of the connected phase delays.

| Angular separations[a] | | |
|---|---|---|
| A–B | $\Delta\alpha$ | $-1^{h}27^{m}\ 2\overset{s}{.}811256\pm0\overset{s}{.}000062$ |
| | $\Delta\delta$ | $4°\ 30'\ 2\overset{''}{.}44833\ \pm0\overset{''}{.}00012$ |
| B–C | $\Delta\alpha$ | $-0^{h}37^{m}42\overset{s}{.}503305\pm0\overset{s}{.}000033$ |
| | $\Delta\delta$ | $-3°\ 54'41\overset{''}{.}67756\ \pm0\overset{''}{.}00013$ |
| C–A | $\Delta\alpha$ | $2^{h}\ 4^{m}45\overset{s}{.}314561\pm0\overset{s}{.}000052$ |
| | $\Delta\delta$ | $-0°\ 35'20\overset{''}{.}77077\ \pm0\overset{''}{.}00013$ |

[a] Estimated errors are based on the combination of the various standard errors included in the analysis: statistical standard errors, and estimated standard errors in the values of the (fixed) parameters of the theoretical model, in the ionospheric model from TEC measurements, and in the reference point chosen for each map. See text and Tables 3 and 4. Correlations among the estimated coordinates for sources A and C, and among the sensitivities of those estimates to the parameters listed in Table 3, have been taken into account in computing the standard errors of the C-A separation.

**Table 3.** Contributions $\delta\Delta\alpha$ and $\delta\Delta\delta$ to the standard errors of the estimates of the sky coordinates of QSO 1928+738 relative to those of each of the two other radio sources obtained from the error sensitivity study.

| Sensitivity analysis results[a] | | | 1803+784 | | 2007+777 | |
|---|---|---|---|---|---|---|
| Parameter | | Standard deviation | $\delta\Delta\alpha$ [$\mu$as][b] | $\delta\Delta\delta$ [$\mu$as] | $\delta\Delta\alpha$ [$\mu$as][b] | $\delta\Delta\delta$ [$\mu$as] |
| Coordinates | $\alpha$ | 145 $\mu$as[b] | 30 | 53 | 35 | 24 |
| of 1928+738[c] | $\delta$ | 280 $\mu$as | 96 | 20 | 47 | 12 |
| Tropospheric | B | 0.1 ns | 105 | 20 | 22 | 105 |
| delay | F | 0.1 ns | 48 | 27 | 22 | 14 |
| at the zenith | P | 0.1 ns | 30 | 22 | 22 | 6 |
| of the radio | T | 0.1 ns | 12 | 9 | 22 | 7 |
| telescopes | X | 0.1 ns | 27 | 23 | 19 | 7 |
| | B | 2 cm | 60 | 62 | 41 | 40 |
| Radio | F | 2 cm | 27 | 18 | 16 | 16 |
| telescope | P | 2 cm | 9 | 16 | 13 | 12 |
| coordinates[c] | T | 2 cm | 12 | 18 | 9 | 10 |
| | X | 2 cm | 33 | 15 | 13 | 13 |
| Earth | x | 1 mas | 3 | 2 | 0 | 1 |
| pole[c] | y | 1 mas | 0 | 0 | 0 | 1 |
| UT1-UTC[c] | | 0.04 ms | 33 | 60 | 38 | 27 |
| rss[d] (estimated standard error) | | | **179** | **118** | **98** | **123** |

[a] Each entry in the last four columns was obtained by altering the a priori value of the parameter in turn by one standard deviation and repeating the least-squares analysis with the resultant table entry being the absolute value of the difference between each result and the "nominal" one.
[b] We use the factor $15\cdot\cos\delta$ to convert $\mu$s to $\mu$as, where $\delta$ is the declination of the radio source.
[c] Standard deviations are twice the values published in IERS (1994) (see Table 1).
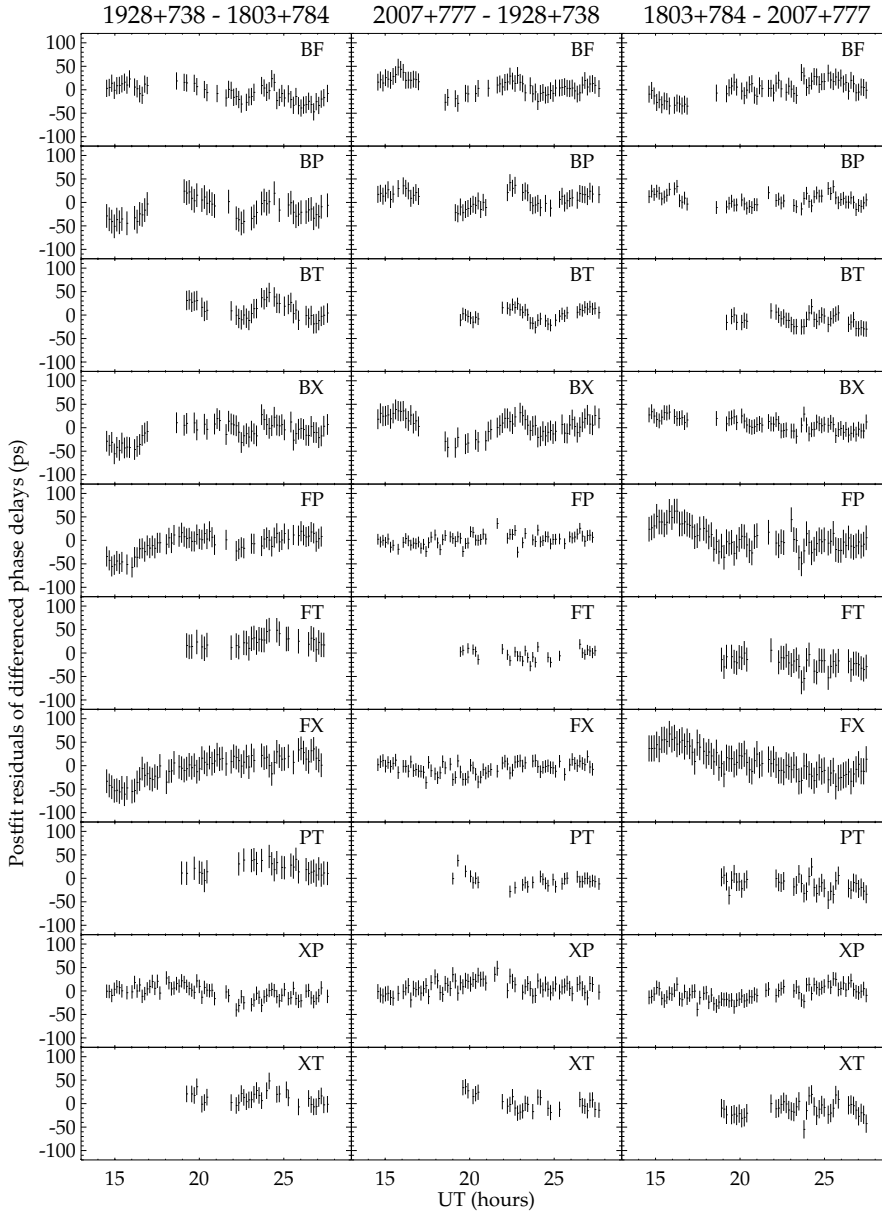[d] The root-sum-square (rss) of the values in the corresponding columns.

**Fig. 4.** Postfit residuals of the differenced phase delays for all baselines and source pairs involved in our analysis (see text). Full (vertical) scale is $\pm$ one phase cycle ($\pm 2\pi$ equivalent), i.e., $\pm 119\,$ps.

components of the relative position between the radio sources as the root-sum-square (rss) of the standard deviations of all the contributions discussed above (see Tables 3 and 4).

We define "sky closure" as the sums of the components of the separation vectors between the three radio sources determined pairwise. For right ascension $\alpha$, we have: $\mathcal{C}_\alpha \equiv \sum \Delta\alpha = \Delta\alpha_{(C\,-\,B)} + \Delta\alpha_{(B\,-\,A)} + \Delta\alpha_{(A\,-\,C)}$, where A, B, and C stand, respectively, for BL 1803+784, QSO 1928+738, and BL 2007+777. Closure in declination $\delta$ is defined correspondingly. The results of the sky-closure test are $\mathcal{C}_\alpha = -66 \pm 360\,\mu$as and $\mathcal{C}_\delta = 15 \pm 220\,\mu$as, that is, zero to well within the indicated standard errors. We estimated these errors as the root-sum-square of the standard errors of the determinations of the pairwise separations. Consequently, these sky closure errors are upper bounds since we ignored the correlations among the pairwise estimates of separation.

## 6. The pair QSO 1928+738/BL 2007+777: registrations and proper motions

We have obtained the pairwise separations among the radio sources BL 1803+784, QSO 1928+738, and BL 2007+777 from observations taken on 20-21 November 1991 through a weighted-least-squares analysis of undifferenced and differenced, connected, nearly ionosphere- and structure-free phase-delays, $\tau_\phi$.

Considering previous observations in addition to ours, we investigated apparent changes in the relative positions of brightness features in the sources QSO 1928+738 and BL 2007+777. These radio sources were previously observed astrometrically in 1985.77 (Guirado et al. 1995a) and 1988.83 (Guirado et al. 1998). For them, we can compare the estimated separations for the three epochs. This comparison is shown in Table 5 and Fig. 5. For each epoch, the reference position for each source is the peak

**Table 4.** Error contributions to the three radio source positions obtained from phase delays.

| | 1803+784 | | 1928+738 | | 2007+777 | |
| | $\delta\Delta\alpha$ | $\delta\Delta\delta$ | $\delta\Delta\alpha$ | $\delta\Delta\delta$ | $\delta\Delta\alpha$ | $\delta\Delta\delta$ |
| Cause | $[\mu\text{as}]^a$ | $[\mu\text{as}]$ | $[\mu\text{as}]^a$ | $[\mu\text{as}]$ | $[\mu\text{as}]^a$ | $[\mu\text{as}]$ |
|---|---|---|---|---|---|---|
| Statistical standard error | 12 | 11 | $-^b$ | $-^b$ | 12 | 9 |
| Fixed parameters in astrometric model[c] | 179 | 118 | $-^b$ | $-^b$ | 98 | 123 |
| Reference point in the map[d] | 14 | 14 | 23 | 12 | 23 | 12 |
| TEC[e] | 42 | 21 | $-^b$ | $-^b$ | 16 | 14 |
| rss (estimated standard error) | **186** | **121** | **23** | **12** | **103** | **125** |

[a] We use the factor $15 \cdot \cos\delta$ to convert $\mu$s to $\mu$as, where $\delta$ is the declination of the radio source.
[b] We took QSO 1928+738 as reference and estimated the positions of the other two sources relative to the position of this reference.
[c] See Table 3.
[d] Each tabulated value includes the estimated standard error in determining the peak of brightness due to the noise in the map and an additional contribution equal in magnitude to the differences between the location of this peak and that of the centroid of the brightest pixel (see text).
[e] The tabulated values are deduced from a sensitivity analysis for an estimated TEC standard error of $1.5 \times 10^{16}$ el/m$^2$ at each site; we assume that the TEC errors for each site are uncorrelated with those for the other sites.
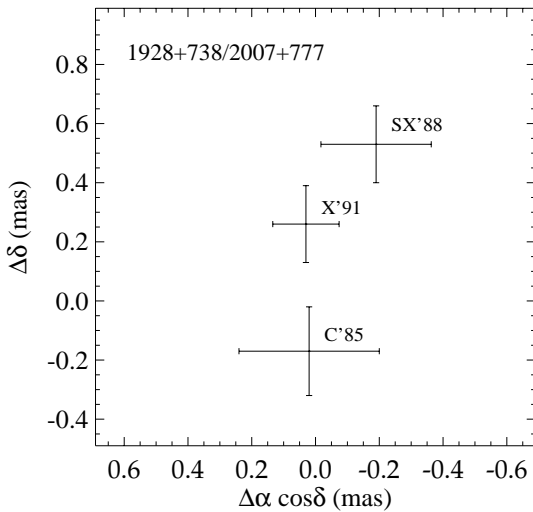


**Fig. 5.** The estimates of the coordinates of QSO 1928+738 minus those of BL 2007+777 (see Table 5). The origin is chosen as in Table 5. Points are labeled to indicate the frequency band(s) used for phase-delay astrometry and the year of each epoch. S corresponds to 2.3 GHz, C to 5 GHz, and X to 8.4 GHz. SX indicates that both S and X bands were used simultaneously.

of brightness of the corresponding map. Our result from epoch 1991.89 lies between the results from the epochs 1985.77 and 1988.83.

We can obtain some insight into this result by investigating the alignment of the maps. The jets of QSO 1928+738 and BL 2007+777 are oriented nearly orthogonally on the sky: The jet of QSO 1928+738 is directed to the south and that of BL 2007+777 to the west. This near orthogonality of the structures was one of the reasons we selected this pair. Indeed, if the cores of the radio sources are assumed stationary as in the standard model, the motions in right ascension and declination of the jet components can be studied without confusion, using only the differenced astrometric results. Alternatively, any apparent motion between the cores that cannot be plausibly as-

signed to some other cause must bring the standard model into question and/or the identification of the core. For example, the possible emission of a new, unresolved component along a jet direction could change the position of the peak of brightness of the corresponding radio source.

An ejection of a component in QSO 1928+738 might imply a declination-oriented shift of the peak of brightness and might affect the difference in declination between this radio source and BL 2007+777, but it would be unlikely to affect significantly the difference in right ascension. A similar analysis holds for BL 2007+777. Therefore, we interpret the predominantly north-south changes (see Table 5) in the separation of QSO 1928+738 and BL 2007+777 between these epochs as shifts with respect to the chosen reference position which are caused by changes in the structure of QSO 1928+738. In other words, the chosen reference position is not the (center of the) true core. In this scenario, the maps of QSO 1928+738 are responsible for all changes: shifts of –170, 530, and 260 $\mu$as in declination, and 20, −190, and 30 $\mu$as in right ascension for epochs 1985.77, 1988.83, and 1991.89, respectively. Accordingly, the corresponding alignment of the maps of BL 2007+777 (Fig. 6) shows no change in the position of the chosen reference point. The maps have been overresolved to show more sharply the reference points chosen, which have been placed at the origins of the maps. We show in Fig. 7 the steps followed to align the maps of QSO 1928+738 and the resulting registration. On the top, we have the three maps aligned at the peaks of brightness as originally determined. In the middle we show the result of shifting those maps based on the results from astrometry and the assumption of no core motion in BL 2007+777. At the bottom, we show the same alignment but with the images overresolved to sharpen the distinction between the components, albeit at the risk of being misled by the overresolution.

The remarkable lack of flux density from the northernmost part of the maps from the first and third epochs, compared to that from the second is hard to understand and represents a clear puzzle in this scenario. Further, it is difficult to understand the proposed shift, with respect to the relative-position refer-

**Table 5.** Estimates at each of three epochs of the J2000.0 coordinates, $\Delta\alpha$ and $\Delta\delta$, of QSO 1928+738 minus those of BL 2007+777[a].

| Epoch | Antennas[b] | Frequency [GHz] | $\Delta\alpha + 37^m 42{.}^s 503330$[a] [ms] | [mas][c] | $\Delta\delta + 3°54'41{.}''67780$[a] [mas] |
|---|---|---|---|---|---|
| 1985.77 | B,L,F,K,O | 5 | 0.005±0.053 | 0.02±0.22 | −0.17±0.15 |
| 1988.83 | B,L,F,M,t | 8.4&2.3 | −0.045±0.042 | −0.19±0.17 | 0.53±0.13 |
| 1991.89 | B,F,P,T,X | 8.4 | 0.008±0.025 | 0.03±0.10 | 0.26±0.13 |

[a] Since we assign the shifts in the separation between the two radio sources to QSO 1928+738, we present here the results obtained estimating the position of QSO 1928+738, while that of BL 2007+777 is held fixed at $\alpha = 20^h 05^m 30{.}^s 998546$, $\delta = 77°52'43{.}''24777$ (IERS 1994). The reference relative coordinates are the same as in Guirado et al. (1998).

[b] The symbols correspond to the following antennas (with diameter and location given in parentheses): B, Effelsberg (100 m, Germany); L, Medicina (32 m, Italy); K, Haystack (37 m, Massachusetts); O, Owens Valley (40 m, California); M, DSS63 (70 m, Spain); F, Fort Davis (25 m, Texas); P, Pie Town (25 m, New Mexico); t, Onsala (20 m, Sweden); T, Kitt Peak (25 m, Arizona); X, Los Alamos (25 m, New Mexico).

[c] To facilitate comparisons between the values of $\Delta\alpha$ and $\Delta\delta$ in the table, we used the factor $15\cdot\cos\delta$, where $\delta$ is the declination of QSO 1928+738, to convert ms to mas.
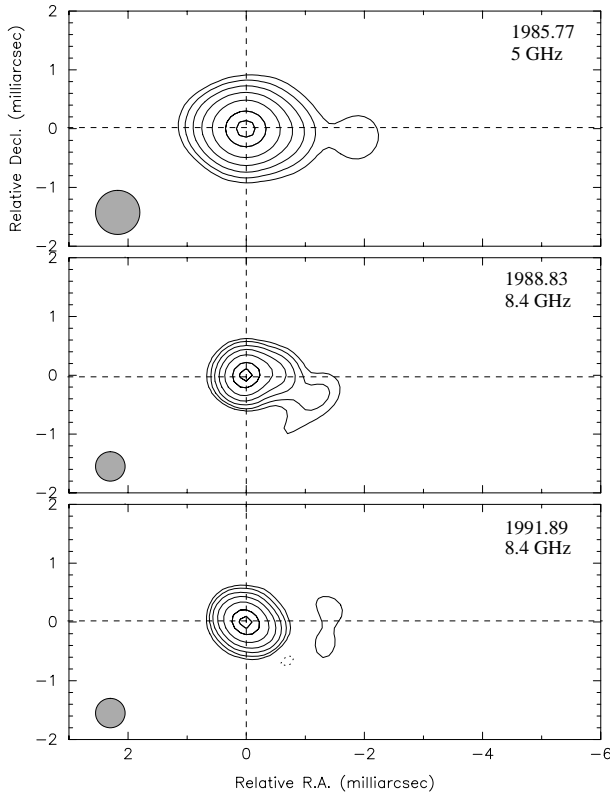


**Fig. 6.** Alignment of the maps of BL 2007+777 based on the astrometric results. Maps are overresolved and contours represent from 2 to 90% of the peak of brightness. Convolving beams (shown at left on each map) are circular, with diameters of 0.75, 0.5, and 0.5 mas, top to bottom. The crossings of the dashed lines show the reference points used in the astrometry. The apparent differences in separation at different epochs between the two radio sources QSO 1928+783 and BL 2007+777 have been entirely attributed to QSO 1928+738 in this scenario (see text).

ence shown in Table 5, in the alignment (Fig. 7) of the maps of QSO 1928+738 from 1985.77 and 1988.83 in terms of a motion of particular features in the map (Guirado et al. 1998), another weakness in this scenario. Nevertheless, following through, we compare these two maps with that from 1991.89 and conclude tentatively that at each of the three epochs the core is centered

about 1.5–2 mas north of the previously chosen reference point. This new identification of the core corresponds to the northernmost feature of the 1988.83 map (undetected in this scenario in 1985.77 and 1991.89).

The core of QSO 1928+738 seems to be continually ejecting components, at an estimated mean rate of one every 1.6 years (H92). The shifts displayed in Fig. 5 are correspondingly "explained" in terms of motions of the peak of brightness, due to newly emerging components. In this scenario, we assume that our originally selected reference point corresponded to a different jet component in each map. The changes in the flux distribution over six years, a period in which, according to H92, up to four components are likely to have emerged, might well have caused the peak of brightness to have moved during this period. For the 1985.77 map at 5 GHz, a difference in the location of the peak of brightness and that of the core of the radio source could also be due in part to opacity effects, but with a value for the shift likely to be less than 0.2 mas (applying a dependence with $k\lambda^\beta$ (Marcaide et al. 1985), with $0.7 < \beta < 2$, and $k$ corresponding to 0.7 mas for $\lambda3.6–13$ cm, we obtain 0.10 mas ($\beta = 2$) to 0.21 mas ($\beta = 0.7$) for $\lambda3.6–6$ cm). This upper limit is small compared with the apparent astrometric shift.

A comparison of this Fig. 5 alignment with the results provided by H92 provides new insights into the problem. H92 identified the core of QSO 1928+738 as the northernmost (and most compact) component of the maps at 22 GHz, based on a 5 year monitoring program. These authors reported that this core had a flat spectrum, because of the similar 8.4 and 22 GHz results. Thus H92 aligned their maps with this core to determine the proper motions of the jet components that they reported. They also developed a model for the kinematics of the jet components involving superluminal motion along a southward traveling sinusoidally curved jet ridge line. In the model this path results from a 2.9 year period of precession of a binary black hole system that would produce a sine function in the maps with a "wavelength" of about 1.06 mas and an "amplitude" of about 0.09 mas. This predicted amplitude (in right ascension) is of the same order of magnitude as the standard error of our astrometric results. The set of components in the H92 model defines a "traveling sine wave" moving at 0.28±0.05 mas/yr, with no sig-
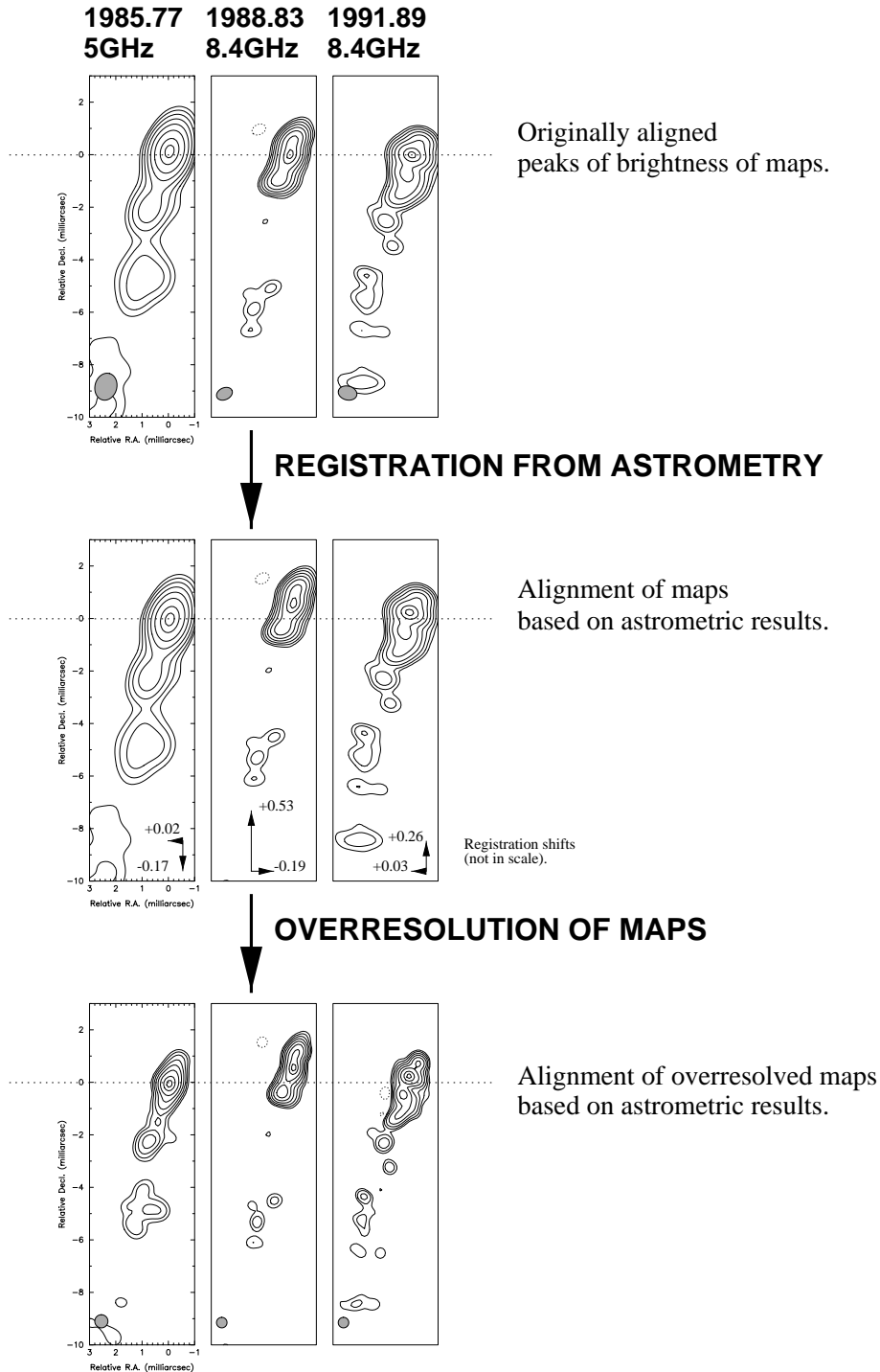
**Fig. 7.** Illustration of steps followed to try to properly align the maps. The astrometric shifts in milliarcseconds are represented (not to scale) at the bottom of the middle figures. The horizontal dotted line in the middle figures passes through the new map origin. The astrometric shifts are the displacements from the origins originally chosen for the maps (upper figures) to the new origins derived from astrometry (see Table 5).

nificant motions of the components with respect to that of the sine wave.

Our observations do not reach the resolution obtained by H92, due primarily to our almost threefold lower radio frequency. We therefore cannot discern the inner structure of the radio sources in as much detail as H92, but we have been able to follow the changes in location of the brightest features by means of our astrometry. By overresolving our map and the maps of Guirado et al. (1998), we tried to identify the components previously reported by H92. Specifically, we inferred that four jet components were emitted between our first and third sets of observations, consistent with the results and predictions of H92. These four components are labeled from south to north in Fig. 8 as A0, A1, A2, and A3.

A0 is identified tentatively as the oldest of these new components (this component was labeled B by H92, as indicated in the upper part of Fig. 8). A0 can also be identified in the maps of 1988.83 and 1991.89 in Fig. 8. It is fainter in these two maps than
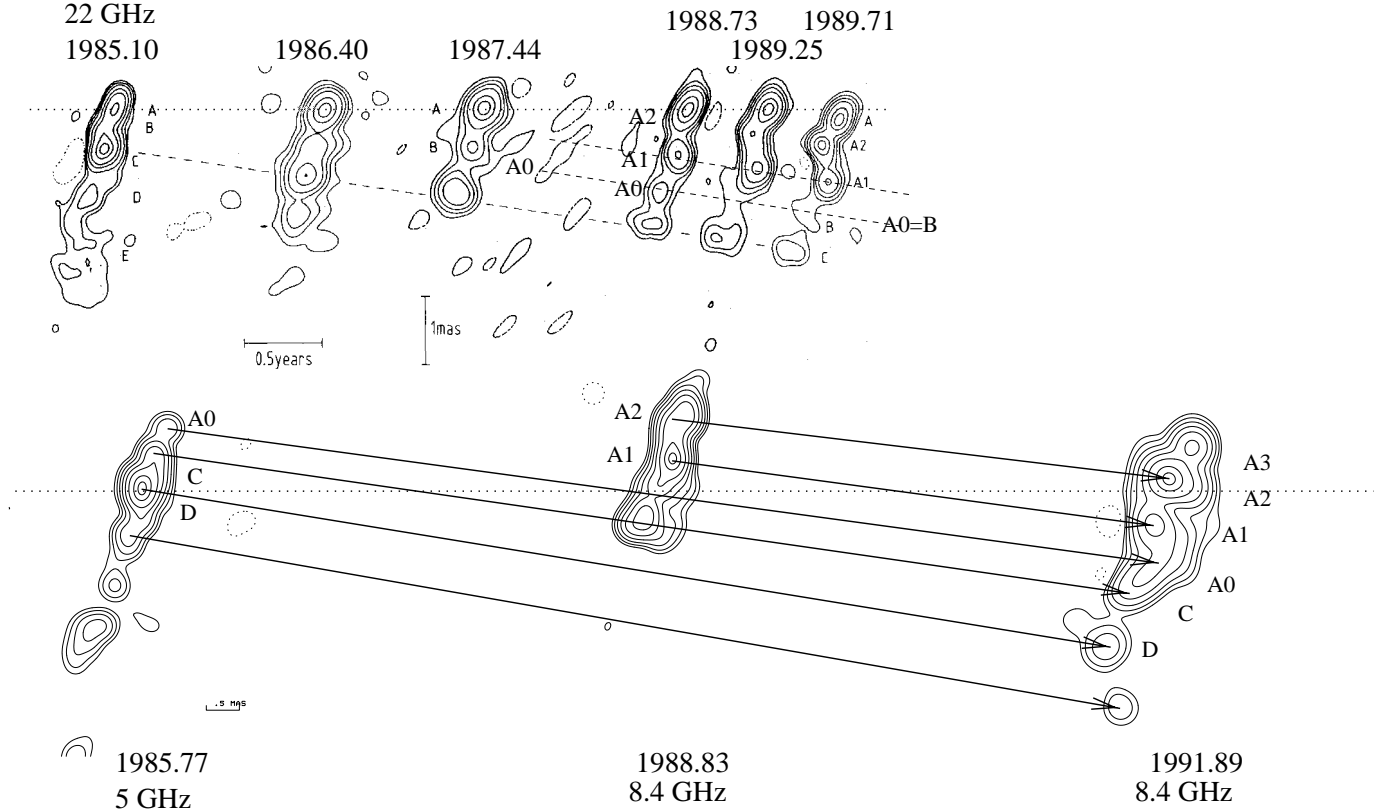
**Fig. 8.** Comparison, on the same angular size and temporal scales, of our results and those of H92 on QSO 1928+738. At the top, maps from H92's 22 GHz observations restored with circular restoring beams of 0.25, 0.30, 0.30, 0.25, 0.25, and 0.25 mas diameter, respectively (left to right). At the bottom, maps from our alignment, with restoring beams of 0.3, 0.3, and 0.4 mas diameter (left to right). We propose identifications of corresponding features and components: For example, H92's C can be identified at 1985.77 and 1991.89. The maps at 1988.73 (this paper) and 1988.83 (H92) show similar features. We also propose identifications of components A1 and A2 in both sets of maps. The dashed and solid lines indicate the proper motions of the components. The horizontal (dotted) lines are drawn for reference.

**Table 6.** Position[a] and proper motions of components in the maps of QSO 1928+738.

|    | Epoch | | | |
|----|------------------------|------------------------|------------------------|------------------------|
|    | 1985.77<br>5 GHz<br>[mas] | 1988.83<br>8.4 GHz<br>[mas] | 1991.89<br>8.4 GHz<br>[mas] | Proper<br>motion<br>[mas/yr] |
| A2 | —            | $-1.09\pm0.10$ | $-0.25\pm0.10$ | $0.27\pm0.05$ |
| A1 | —            | $-0.53\pm0.10$ | $0.45\pm0.15$  | $0.32\pm0.05$ |
| A0 | $-1.12\pm0.30$ | $-0.06\pm0.15$ | $0.98\pm0.15$  | $0.34\pm0.05$ |
| C  | $-0.49\pm0.15$ | $0.44\pm0.10$  | $1.43\pm0.15$  | $0.32\pm0.03$ |
| D  | $0.08\pm0.15$  | —            | $2.31\pm0.15$  | $0.36\pm0.04$ |

[a] Angular distances of components are given with respect to the origin chosen, based on the astrometric alignment of the maps (see text and Fig. 7).

in the one of 1985.77. Our estimate of its proper motion, based on our conjectured astrometric alignment, is $0.34\pm0.05$ mas/yr, with the quoted error being the statistical standard error (see Table 6).

A1 is a component that emerged between 1985.77 and 1988.83. It corresponds to the peak of brightness in the map of 1988.83 and can also be identified in the 1991.89 map, yielding an estimated proper motion of $0.32\pm0.05$ mas/yr (see Table 6).

A2 emerged later and represents the peak of brightness in the 1991.89 map; in 1988.83 it had been near our initially assumed position of the core. Our estimate of its proper motion is $0.27\pm0.05$ mas/yr (see Table 6).

The newest component, A3, apparently emerged after the 1988.83 epoch. It is, we believe, south of the position of the (undetected) core, but, of course, north of the rest of the structure.

Component C marked in the H92 maps can be identified in our maps at 5 and 8.4 GHz. The different relative brightnesses of components C and D in the 22 and 5 GHz maps of 1985 might be due to C having still been self-absorbed at 5 GHz while D was already in the optically thin phase of its evolution. Our estimate of the proper motion of component C from the three maps is $0.32\pm0.03$ mas/yr (see Table 6).

It is remarkable that D is not visible in the 1988.83 map, even though it is the brightest feature of the 1985.77 image. Similarly, C is at least twofold brighter and also more extended in the 1988.83 map than we would have expected from its evolution along a jet. The brightness change and the extension change can perhaps be explained by the undersampling of the $(u, v)$

plane for intermediate spatial frequencies. Table 5 shows that the array at this epoch consisted of four European radio telescopes and one in the U.S. (Fort Davis). This array provided sampling only at 30-50 M$\lambda$ for six baselines and at about 200 M$\lambda$ for the four intercontinental ones. Intermediate spatial frequencies were not sampled. Hybrid mapping could have assigned to the inner features the flux density of these undetected components, as model fitting confirms. Specifically, for this poor sampling of those intermediate spatial frequencies, the visibilities of the map from Guirado et al. (1998) are essentially equivalent to those generated by a model, consisting of elliptical Gaussian components fit to the observed visibility data, that includes a component located where we believe component D is located. The other components of the model were located as found in the hybrid maps. The proper motion of component D, deduced from only our first and third epochs, is 0.36±0.04 mas/yr (statistical standard error).

Our proper motion results agree with those reported by H92. Although we have lower resolution data than they, we took advantage of our ability to align the maps of QSO 1928+738 based on our accurate astrometric results, to obtain a longer time base.

## 7. Conclusions

We have shown that at 8.4 GHz phase delays can be "connected" reliably for sources 7° apart on the sky even at epochs of maximum solar activity. Guirado et al. (1995a) and Lara et al. (1996) demonstrated such phase connection for angular distances of ∼5°, but not for epochs of high solar activity and rapidly varying TEC. Here, under such conditions, we succeeded at phase connection with 8.4 GHz, but not with 2.3 GHz data.

We removed most of the structure phase from the astrometric observables based on the hybrid maps obtained from our observations and the selection of reference points in the maps, as in the past. Nevertheless, errors at the milliarcsecond level in the comparison of astrometric positions determined from data obtained at different epochs can result from changes in the structures of the radio sources, if such changes are not taken into account properly. We try to diminish such error or bias, by attempting to remove the effects of the source structure from our data through referring all astrometric measurements to the core (i.e., the same "physical" point) in the source.

As a possible improvement to the general astrometric technique, we removed most of the effect of the ionosphere by means of TEC estimates deduced from GPS measurements at stations in the vicinity of the radio telescopes that we used. This important step forward is vital when adequate dual-band VLBI observations are not available. Moreover, given sufficiently accurate corrections for ionospheric effects from GPS measurements, only single-band VLBI observations need to be performed so that higher sensitivity (e.g., for fainter sources) can be obtained by using the whole recording bandwidth for this single band. The technical aspects of the procedure will be presented in a complementary paper (Ros et al. 1999).

After obtaining the pairwise relative positions of the three radio sources, we compared the separation of the pair

QSO 1928+738/BL 2007+777 with two previous results from earlier epochs. Our relative position fell between the other two: we interpreted the differences as being due to different "physical" reference points in the sources being used (unintentionally) at the different epochs of observation.

According to H92, QSO 1928+738 is a superluminal radio source that ejects components which seem to move along a sinusoidal trajectory starting at a flat-spectrum component detected at 22 GHz that H92 identified with the core. However, the inferences drawn from what seemed to be the correct alignment of our maps, led us to question this identification, suggesting instead that the core is further north. We then identified four components that emerged during the six years spanned by our observations (late 1985 to late 1991), which we labeled A0, A1, A2, and A3; their proper motions all appear to be in the range of 0.3-0.4 mas/yr.

In the future, the improvements incorporated into our present data reduction can perhaps be successfully applied to radio sources much further apart on the sky and at any part of the solar activity cycle with the use of only single-band observations. In addition, the better performance in recent years of the global VLBI network (especially the VLBA) provides sizable advantages for phase-delay astrometry: higher slew speeds of radio telescopes with corresponding reduction of slew times, better sensitivity of receivers, and automated data correlation with the corresponding reduction of "waiting" times. We believe that far more ambitious projects are now possible.

## References

Antonucci R.R.J., 1986, ApJ 304, 634
Chao C.C., 1972, Tech. Memo Caltech/JPL No. 391-350
Chao C.C., 1974, JPL/NASA Tech. Rep. No. 32-1587, 61
Eckart A., 1983, Untersuchung der Eigenschaften extragalaktischer Radioquellen. Dissertation, Universität Münster, Germany
Eckart A., Witzel A., Biermann P., et al., 1985, ApJ 296, L23
Eckart A., Witzel A., Biermann P., et al., 1986, A&A 168, 17
Eckart A., Witzel A., Biermann P., et al., 1987, A&AS 67, 121
Fricke W., Schwan H., Lederle T., et al., 1988, Fifth fundamental catalogue (FK5). Part 1: The basic fundamental stars. Astronomisches Rechen-Institut, Heidelberg, Germany
Fricke W., Schwan H., Corbin T., et al., 1991, Fifth fundamental catalogue. Part 2: The FK5 extension - new fundamental stars. Astronomisches Rechen-Institut, Heidelberg, Germany

Fomalont E.B., 1989, In: Perley R.A., Schwab F.R., Bridle A.H. (eds.) Synthesis Imaging in Radio Astronomy. A.S.P. Conference Series 6, 213

Guirado J.C., Marcaide J.M., Elósegui P., et al., 1995a, A&A 293, 613

Guirado J.C., Marcaide J.M., Alberdi A., et al., 1995b, AJ 110, 2586

Guirado J.C., Marcaide J.M., Ros E., et al., 1998, A&A 336, 385

Hummel C.A., 1990, Untersuchung ausgewählter Jets extragalaktischer Radioquellen. Dissertation, Rheinisch Friedrich-Wilhelms-Universität zu Bonn, Germany

Hummel C.A., Schalinski C.J., Krichbaum T.P., et al., 1992, A&A 257, 489 (H92)

International Earth Rotation Service (IERS), 1994, In: Feissel M., Essaïfi N. (eds.) Annual Report for 1993, Paris, France

Johnston K.J., Simon R.S., Eckart A., et al., 1987, ApJ 313, L85

Johnston K.J., Fey A.L., Zacharias N., et al., 1995, AJ 110, 880

Klobuchar J.A., 1975, Air Force Cambridge Research Laboratories Report No. AFCRL-TR-75-0502 (NTIS ADA 018862)

Kollgaard R.I., Wardle J.F.C., Roberts D.H., Gabuzda D.C., 1992, AJ 104, 1687

Krichbaum T.P., Booth R.S., Kus A.J., et al., 1990, A&A 237, 3

Krichbaum T.P., Witzel A., Graham D.A., 1993, In: Davies R.J., Booth R.S. (eds.) Subarcsecond Radio Astronomy. Cambridge University Press, 187

Krichbaum T.P., Standke K.J., Graham D.A., et al., 1994a, In: Courvoisier T.J.-L., Blecha R.A. (eds.) Multi-Wavelength Continuum Emission of AGN. Kluwer, Dordrecht, The Netherlands, 187

Krichbaum T.P., Witzel A., Standke K.J., et al., 1994b, In: Zensus J.A., Kellermann K.I. (eds.) Compact Extragalactic Radio Sources. NRAO, Socorro, NM, USA, 39

Kühr H., Witzel A., Pauliny-Toth I.I.K., Nauber U., 1981, A&AS 45, 367

Lara L., Marcaide J.M., Alberdi A., Guirado J.C., 1996, A&A 314, 672

Lawrence C.R., Pearson T.J., Readhead A.C.S., Unwin S.C., 1986, AJ 91, 494

Lieske J.H., Lederle T., Fricke W., 1977, A&A 58, 1

Marcaide J.M., Shapiro I.I., Corey B.E., et al., 1985, A&A 142, 71

Murphy D.W., Browne I.W.A., Perley R.A., 1993, MNRAS 264, 298

Pearson T.J., Readhead A.C.S., 1988, ApJ 328, 114

Pearson T.J., 1991, BAAS 23, 991

Robertson D.S., 1975, Geodetic and Astrometric Measurements with Very-Long-Baseline Interferometry. Ph.D., MIT, Cambridge, MA, USA

Rogers A.E.E., Cappallo R.J., Hinteregger H.F., et al., 1983, Sci 219, 51

Roos N., Kaastra J.S., Hummel C.A., 1993, ApJ 409, 130

Ros E., Marcaide J.M., Guirado J.C., Sardón E., Shapiro I.I., 1999, A&A, in preparation

Rusk R., Rusk A.C.M., 1986, Can. Jou. of Phys. 64, 440

Saastamoinen J., 1973, Bull. Géodésique 105, 279

Sardón E., Rius A., Zarraoa N., 1994, Radio Science 29, 577

Schalinski C.J., 1990, Untersuchungen der Zentralregionen aktiver Galaxienkerne. Dissertation, Friedrich-Wilhelms-Universität zu Bonn, Germany

Shapiro I.I., Wittels J.J., Counselman C.C., et al., 1979, AJ 84, 1459

Shepherd M.C., Pearson T.J., Taylor G.B., 1995, BAAS 26, 987

Steffen W., 1994, Helikale Strukturen in aktiven Galaxienkernen. Dissertation, Friedrich-Wilhelms-Universität zu Bonn, Germany

Stickel M., Padovani P., Urry C.M., Fried J.W., Kühr H., 1991, ApJ 374, 431

Strom R.G., Biermann P.L., 1991, A&A 242, 313

Thompson A.R., Moran J.M., Swenson G.W., 1986, Interferometry and Synthesis in Radio Astronomy. Wiley, New York, NY, USA

Witzel A., Schalinski C.J., Johnston K.J., et al., 1988, A&A 206, 245